Dark solitons near potential and nonlinearity steps

F. Tsitoura, Z. A. Anastassi, J. L. Marzuola, P. G. Kevrekidis, and D. J. Frantzeskakis

Dark solitons near potential and nonlinearity steps

F. Tsitoura,[1] Z. A. Anastassi,[2] J. L. Marzuola,[3] P. G. Kevrekidis,[4, 5] and D. J. Frantzeskakis[1]

[1]*Department of Physics, University of Athens, Panepistimiopolis, Zografos, Athens 15784, Greece*
[2]*Department of Mathematics, Statistics and Physics, College of Arts and Sciences, Qatar University, 2713 Doha, Qatar*
[3]*Department of Mathematics, University of North Carolina, Chapel Hill, NC 27599, USA*
[4]*Department of Mathematics and Statistics, University of Massachusetts, Amherst, Massachusetts 01003-4515 USA*
[5]*Center for Nonlinear Studies and Theoretical Division,*
Los Alamos National Laboratory, Los Alamos, NM 87544

We study dark solitons near potential and nonlinearity steps and combinations thereof, forming rectangular barriers. This setting is relevant to the contexts of atomic Bose-Einstein condensates (where such steps can be realized by using proper external fields) and nonlinear optics (for beam propagation near interfaces separating optical media of different refractive indices). We use perturbation theory to develop an equivalent particle theory, describing the matter-wave or optical soliton dynamics as the motion of a particle in an effective potential. This Newtonian dynamical problem provides information for the soliton statics and dynamics, including scenarios of reflection, transmission, or quasi-trapping at such steps. The case of multiple such steps and its connection to barrier potentials is additionally touched upon. The range of validity of the analytical approximation and radiation effects are also investigated. Our analytical predictions are found to be in very good agreement with the corresponding numerical results, where appropriate.

I. INTRODUCTION

The interaction of solitons with impurities is a fundamental problem that has been considered in various branches of physics – predominantly in nonlinear wave theory [1] and solid state physics [2] – as well as in applied mathematics (see, e.g., recent work [3] and references therein). Especially, in the framework of the nonlinear Schrödinger (NLS) equation, the interaction of bright and dark solitons with δ-like impurities has been investigated in many works (see, e.g., Refs. [4–8]). Relevant studies in the context of atomic Bose-Einstein condensates (BECs) [9–11] have also been performed (see, e.g., Refs. [12–16]), as well as in settings involving potential wells [17, 18] and barriers [19, 20] (see also Ref. [21] for earlier work in a similar model). In this context, localized impurities can be created by focused far-detuned laser beams, and have already been used in experiments involving dark solitons [22, 23]. Furthermore, experimental results on the scattering of matter-wave bright solitons on Gaussian barriers in either ^{7}Li [24] or ^{85}Rb [25] BECs have been reported as well. More recently, such soliton-defect interactions were also explored in the case of multi-component BECs and dark-bright solitons, both in theory [26] and in an experiment [27].

On the other hand, much attention has been paid to BECs with spatially modulated interatomic interactions, so-called "collisionally inhomogeneous condensates" [28, 29]; for a review with a particular bend towards periodic such interactions see also Ref. [30]). Relevant studies in this context have explored a variety of interesting phenomena: these include, but are not limited to adiabatic compression of matter-waves [28, 31], Bloch oscillations of solitons [28], emission of atomic solitons [32, 33], scattering of matter waves through barriers [34], emergence of instabilities of solitary waves due to periodic variations in the scattering length [35], formation of stable condensates exhibiting both attractive and repulsive interatomic interactions [36], solitons in combined linear and nonlinear potentials [37–41], generation of solitons [42] and vortex rings [43], control of Faraday waves [44], vortex dipole dynamics in spinor BECs [45], and others.

Here, we consider a combination of the above settings, namely we consider a one-dimensional (1D) setting involving potential and nonlinearity steps, as well as pertinent rectangular barriers, and study statics, dynamics and scattering of dark solitons. In the BEC context, recent experiments have demonstrated robust dark solitons in the quasi-1D setting [46]. In addition, potential steps in BECs can be realized by trapping potentials featuring piece-wise constant profiles (see, e.g., Refs. [47, 48] and discussion in the next Section). Furthermore, nonlinearity steps can be realized too, upon employing magnetically [49] or optically [50] induced Feshbach resonances, that can be used to properly tune the interatomic interactions strength – see, e.g., more details in Refs. [33, 38] and discussion in the next Section.

Such a setting involving potential and nonlinearity steps, finds also applications in the context of nonlinear optics. There, effectively infinitely long potential and nonlinearity steps of constant and finite height, describe interfaces separating optical media characterized by different linear and nonlinear refractive indices [51]. In such settings, it has been shown [52–55] that the dynamics of self-focused light channels – in the form of spatial bright solitons – can be effectively described by the motion of an equivalent particle in effective step-like potentials. This "equivalent particle theory" actually corresponds to the adiabatic approximation of the perturbation theory of solitons [1], while reflection-induced radiation effects can be described at a higher-order approximation [53, 54]. Note that similar studies, but for dark solitons in settings involving potential steps and rectangular barriers, have also been performed – see, e.g., Ref. [56] for an effective particle theory, and Refs. [57–59] for numerical studies of reflection-induced radiation effects. However, to the best of our knowledge, the statics and dynamics of dark solitons

near combined potential and nonlinearity steps, have not been systematically considered so far in the literature, although a special version of such a setting has been touched upon in Ref. [38]. In a recent study [60], vortex dynamics in the $2D$ Gross-Pitaevskii equation was considered and it was observed that true jumps in the barriers were quite difficult to deal with, by using techniques available there, and that some more regularity was required to derive a particle like picture for vortex dynamics. It is thus rather interesting that dark solitons can still be handled in such a setting, provided the jumps are not too large as will be quantified later.

It is our purpose, in this work, to address this problem. In particular, our investigation and a description of our presentation is as follows.

First, in Sec. II, we provide the description and modeling of the problem; although this is done in the context of atomic BECs, our model can straightforwardly be used for similar considerations in the context of optics, as mentioned above. In the same Section, we apply perturbation theory for dark solitons to show that, in the adiabatic approximation, soliton dynamics is described by the motion of an equivalent particle in an effective potential. The latter has a tanh-profile, but – in the presence of the nonlinearity step – can also exhibit a minimum and a maximum, i.e., an elliptic and a hyperbolic fixed point, respectively, in the effective dynamical system. We show that stationary soliton states do exist at the fixed points, but are unstable (albeit in different ways, as is explained below) according to a Bogoliubov-de Gennes (BdG) analysis [9–11] that we perform; we also use an analytical approximation to derive the unstable eigenvalues as functions of the magnitudes of the potential/nonlinearity steps.

In Sec. III we study the soliton dynamics for various parameter values, pertaining to different forms of the effective potential, including the case of rectangular barriers formed by a combination of adjacent potential and nonlinearity steps. Our numerical results – in both statics and dynamics – are found to be in very good agreement with the analytical predictions. We also investigate the possibility of soliton trapping in the vicinity of the hyperbolic fixed point of the effective potential; note that such states could be characterized as "surface dark solitons", as they are formed at linear/nonlinear interfaces separating different optical or atomic media. We show that quasi-trapping of solitons is possible, in the case where nonlinearity steps are present; the pertinent (finite) trapping time is found to be of the order of several hundreds of milliseconds, which suggests that such soliton quasi-trapping could be observable in real BEC experiments.

In Sec. IV we extend our considerations beyond the perturbative regime and study, in particular, soliton scattering at larger potential and nonlinearity steps. Our investigation reveals both the range of validity of our analytical approximation and the role of the emission of radiation – in the form of sound waves – during the scattering process. We find that, generally, when the soliton moves from a region of larger towards a region of smaller background density, and is scattered at the discontinuity, then the soliton energy and number of atoms decrease. The process is such that the difference between initial and final values of the energy and number of atoms is equal to the radiation's respective quantities. Our pertinent numerical results also reveal the range of validity of our analytical approach: the latter remains accurate as long as the percentage strengths of potential/nonlinearity steps are of the order of 10% of the respective background values, and fails for larger strengths.

Finally, in Sec. V we summarize our findings, discuss our conclusions, and provide perspectives for future studies.

II. MODEL AND ANALYTICAL CONSIDERATIONS

A. Setup

As noted in the Introduction, our formulation originates from the context of atomic BECs in the mean-field picture [9]. We thus consider a quasi-1D setting whereby matter waves, described by the macroscopic wave function $\Psi(x, t)$, are oriented along the x-direction and are confined in a strongly anisotropic (quasi-1D) trap. The latter, has the form of a rectangular box of lengths $L_x \gg L_y = L_z \equiv L_\perp$, with the transverse length $L_\perp$ being on the order of the healing length ξ. Such a box-like trapping potential, $V_b(x)$, can be approximated by a super-Gaussian function, of the form:

$$V_b(x) = V_0 \left[1 - \exp\left(-\left(\frac{x}{w}\right)^\gamma \right) \right], \quad (1)$$

where V_0 and w denote the trap amplitude and width, respectively. The particular value of the exponent $\gamma \gg 1$ is not especially important; here we use $\gamma = 50$. In this setting, our aim is to consider dark solitons near potential and nonlinearity steps, located at $x = 0$. To model such a situation, we start from the Gross-Pitaevskii (GP) equation [9, 10]:

$$i\hbar \frac{\partial \Psi}{\partial t} = \left[-\frac{\hbar^2}{2m} \frac{\partial^2}{\partial x^2} + g_{1D}(x)|\Psi|^2 + V(x) \right] \Psi, \quad (2)$$

Here, $\Psi(x, t)$ is the mean-field wave function, m is the atomic mass, $V(x)$ represents the external potential, while $g_{1D}(x) = (9/4L_\perp^2)g_{3D}(x)$ is the effectively 1D interaction strength, with $g_{3D} = 4\pi\hbar^2\alpha(x)/m$ being its 3D counterpart and $\alpha(x)$ being the scattering length (assumed to be $\alpha > 0$, $\forall x$, corresponding to repulsive interatomic interactions). The external potential and the scattering length are then taken to be of the form:

$$V(x) = V_b(x) + \begin{cases} V_L, & x < 0 \\ V_R, & x > 0 \end{cases}, \quad (3)$$

$$\alpha(x) = \begin{cases} \alpha_L, & x < 0 \\ \alpha_R, & x > 0 \end{cases}, \quad (4)$$

where $V_{L,R}$ and $\alpha_{L,R}$ are constant values of the potential and scattering length, to the left and right of $x = 0$, where respective steps take place (subscripts L and R stand for "Left" and "Right", respectively).

Notice that such potential steps may be realized in present BEC experiments upon employing a detuned laser beam

shined over a razor edge to make a sharp barrier, with the diffraction-limited fall-off of the laser intensity being smaller than the healing length of the condensate; in such a situation, the potential can be effectively described by a step function. On the other hand, the implementation of nonlinearity steps can be based on the interaction tunability of specific atomic species by applying external magnetic or optical fields [49, 50]. For instance, confining ultracold atoms in an elongated trapping potential near the surface of an atom chip [61] allows for appropriate local engineering of the scattering length to form steps (of varying widths), where the atom-surface separation sets a scale for achievable minimum step widths. The trapping potential can be formed optically, possibly also by a suitable combination of optical and magnetic fields (see Ref. [38] for a relevant discussion).

Measuring the longitudinal coordinate x in units of $\sqrt{2}\xi$ (where $\xi \equiv \hbar/\sqrt{2mn_{\mathrm{L}}g_{\mathrm{1D}}}$ is the healing length), time t in units of $\sqrt{2}\xi/c_s^{(\mathrm{L})}$ (where $c_s^{(\mathrm{L})} \equiv \sqrt{g_{\mathrm{1D}}n_{\mathrm{L}}/m}$ is the speed of sound and n_{L} is the density of the ground state for $x < 0$), and energy in units of $g_{\mathrm{1D}}n_{\mathrm{L}}$, we cast Eq. (2) to the following dimensionless form (see Ref. [62]):

$$i\frac{\partial u}{\partial t} = -\frac{1}{2}\frac{\partial^2 u}{\partial x^2} + \frac{\alpha(x)}{\alpha_{\mathrm{L}}}|u|^2 u + V(x)u, \qquad (5)$$

where $u = \sqrt{n_{\mathrm{L}}}\Psi$. Here we should mention that Eq. (5) can also be applied in the context of nonlinear optics [51]: in this case, u represents the complex electric field envelope, t is the propagation distance and x is the transverse direction, while $V(x)$ and $\alpha(x)$ describe the (transverse) spatial profile of the linear and nonlinear parts of the refractive index [39]. This way, Eq. (5) can be used for the study of optical beams, carrying dark solitons, near interfaces separating different optical media, with (different) defocusing Kerr nonlinearities.

B. Perturbation theory and equivalent particle picture

Assuming that, to a first approximation, the box potential can be neglected, we consider the dynamics of a dark soliton, which is located in the region $x < 0$, and moves to the right, towards the potential and nonlinearity steps at $x = 0$ (similar considerations for a soliton located in the region $x > 0$ and moving to the left are straightforward). In such a case, we seek for a solution of Eq. (5) in the form:

$$u(x, t) = \sqrt{\mu_{\mathrm{L}} - V_{\mathrm{L}}} \exp\left(-i\mu_{\mathrm{L}}t\right)v(x, t), \qquad (6)$$

where μ_{L} is the chemical potential, and $v(x, t)$ is the wavefunction of the dark soliton. Then, introducing the transformations $t \to (\mu_{\mathrm{L}} - V_{\mathrm{L}})t$ and $x \to \sqrt{\mu_{\mathrm{L}} - V_{\mathrm{L}}}x$, we express Eq. (5) as a perturbed NLS equation for the dark soliton:

$$i\frac{\partial v}{\partial t} + \frac{1}{2}\frac{\partial^2 v}{\partial x^2} - \left(|v|^2 - 1\right)v = P(v). \qquad (7)$$

Here, the functional perturbation $P(v)$ has the form:

$$P(v) = \left(A + B|v|^2\right)v\mathcal{H}(x), \qquad (8)$$

where $\mathcal{H}$ is the Heaviside step function, and coefficients A, B are given by:

$$A = \frac{V_{\mathrm{R}} - V_{\mathrm{L}}}{\mu_{\mathrm{L}} - V_{\mathrm{L}}}, \quad B = \frac{\alpha_{\mathrm{R}}}{\alpha_{\mathrm{L}}} - 1. \qquad (9)$$

These coefficients, which set the magnitudes of the potential and nonlinearity steps, are assumed to be small. Such a situation corresponds, e.g., to the case where $\mu_{\mathrm{L}} = 1$, $V_{\mathrm{L}} = 0$, $V_{\mathrm{R}} \sim \epsilon$, and $\alpha_{\mathrm{R}}/\alpha_{\mathrm{L}} \sim 1$, where $0 < \epsilon \ll 1$ is a formal small parameter (this choice will be used in our simulations below). In the present work, we assume that the jump from left to right is "sharp", i.e., we do not explore the additional possibility of a finite width interface. If such a finite width was present, but was the same for the potential and nonlinearity steps, essentially the formulation below would still be applicable, with the Heaviside function above substituted by a suitable smoothed variant (e.g. a $\tanh$ functional form). A more complicated setting deferred for future studies would involve the existence of two separate widths in the linear and nonlinear step and the length scale competition that that could involve.

Equation (7) can be studied analytically upon employing perturbation theory for dark solitons (see, e.g., Refs. [63–65]). Here, following the approach of Ref. [63], first we note that, in the absence of the perturbation (8), Eq. (7) has a dark soliton solution of the form:

$$v(x, t) = \cos\phi\tanh X + i\sin\phi, \qquad (10)$$

where $X = \cos\phi[x - x_0(t)]$ is the soliton coordinate, ϕ is the soliton phase angle ($|\phi| < \pi/2$) describing the darkness of the soliton, $\cos\phi$ is the soliton depth ($\phi = 0$ and $\phi \neq 0$ correspond to stationary black solitons and gray solitons, respectively), while $x_0(t)$ and $dx_0/dt = \sin\phi$ denote the position of the soliton center and velocity, respectively. Then, considering an adiabatic evolution of the dark soliton, we assume that in the presence of the perturbation the dark soliton parameters become slowly-varying unknown functions of time t. Thus, the soliton phase angle becomes $\phi \to \phi(t)$ and, as a result, the soliton coordinate becomes $X = \cos\phi(t)\left(x - x_0(t)\right)$, with $dx_0(t)/dt = \sin\phi(t)$.

The evolution of the soliton phase angle can be found by means of the evolution of the renormalized soliton energy, E_s, given by (see Refs. [63, 64] for details):

$$E_s = \frac{1}{2}\int_{-\infty}^{\infty}\left[\left|\frac{\partial v}{\partial x}\right|^2 + \left(|v|^2 - 1\right)^2\right]dx. \qquad (11)$$

Employing Eq. (10), it can readily be found that $dE_s/dt = -4\cos^2\phi\,\sin\phi\,d\phi/dt$. On the other hand, using Eq. (7) and its complex conjugate, yields the evolution of the renormalized soliton energy: $dE_s/dt = -\int_{-\infty}^{+\infty}\left(P\partial\bar{v}/\partial t + \bar{P}\partial v/\partial t\right)dx$, where bar denotes complex conjugate. Then, the above expressions for dE_s/dt yield the evolution of ϕ, namely:

$$\frac{d\phi}{dt} = \frac{1}{2\cos^2\phi\sin\phi}\mathrm{Re}\left\{\int_{-\infty}^{+\infty}P(v)\frac{\partial\bar{v}}{\partial t}dx\right\}. \qquad (12)$$

Inserting the perturbation (8) into Eq. (12), and performing the integration, we obtain the following result:

$$\frac{d\phi}{dt} = -\frac{1}{8}\operatorname{sech}^2(x_0)\left[2(A+B) - B\operatorname{sech}^2(x_0)\right], \quad (13)$$

where we have considered the case of nearly stationary (black) solitons with $\cos\phi \approx 1$ (and $\sin\phi \approx \phi$). Combining Eq. (13) with the above mentioned equation for the soliton velocity, $dx_0(t)/dt = \sin\phi(t)$, we can readily derive the following equation for motion for the position of the soliton center:

$$\frac{d^2 x_0}{dt^2} = -\frac{dW}{dx_0}, \quad (14)$$

where the effective potential $W(x_0)$ is given by:

$$W(x_0) = \frac{1}{24}\tanh(x_0)\left[3(2A+B) + B\tanh^2(x_0)\right]. \quad (15)$$

C. Forms of the effective potential

The form of the effective potential suggests that extrema [and associated fixed points of the dynamical system (14)], where – potentially – dark solitons may be trapped, exist only in the presence of the nonlinearity step ($B \neq 0$). In other words, it is the competition between the linear and nonlinear step that enable the presence of fixed points and associated more complex dynamics. Indeed, in the presence of solely a linear step, the effective potential features the form of a step potential, with no critical points, similarly to what is the case for its bright sibling [21]; see also below.

In fact, in our setting it is straightforward to find that, in general, there exist two fixed points, located at:

$$x_{0\pm} = \frac{1}{2}\ln\left(\frac{-A \mp \sqrt{-B(2A+B)}}{A+B}\right), \quad (16)$$

for $B(2A+B) < 0$, with $-2A < B < -A$ if $A > 0$, and $-A < B < -2A$ if $A < 0$. In Fig. 1 we plot $B(2A+B)$ as a function of B, for $A > 0$ [solid (blue) line] and $A < 0$ [dashed (red) line]. The corresponding domains of existence of extrema in the potential [and, thus, fixed points in the system (14)], are also depicted by the gray areas. Insets show typical profiles of the effective potential $W(x_0)$, for different values of B, which we discuss in more detail below. From the figure (as well as from Eq. (16) itself), the saddle-center nature of the bifurcation of the two fixed points, which are generated concurrently "out of the blue sky" is immediately evident.

First, we consider the case of the absence of the nonlinearity step, $B = 0$, as shown in the insets I and IV of Fig. 1, for $A > 0$ and $A < 0$, respectively. In this case, $W(x_0)$ assumes a step profile, induced by the potential step. If, in addition, a nonlinearity step is present, so that parameter B lies in the interval $-A < B < 0$ or $0 < B < -A$, in the cases $A > 0$ or $A < 0$ respectively, then the potential $W(x_0)$ assumes again a step profile, but its asymptotes (for $x_0 \to \pm\infty$) become slightly smaller.
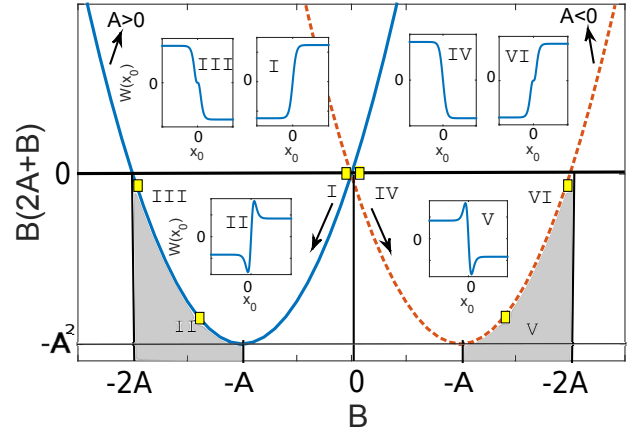

FIG. 1: Sketch showing domains of existence of extrema of the effective potential $W(x_0)$, i.e., fixed points of the dynamical system (14), depicted by gray areas, for $A > 0$ [solid (blue) line] and $A < 0$ [dashed (red) line]. The insets $I - III$ ($IV - VI$) show the form of $W(x_0)$, starting from $B = 0$ (insets I and IV) and ending to a small finite value of B, which is gradually decreased (increased) for $A > 0$ ($A < 0$), cf. black arrows. Rectangular (yellow) points indicate parameter values corresponding to the forms of $W(x_0)$ shown in the insets $I - VI$.

A more interesting situation occurs when the nonlinearity step takes on the values $-2A < B < -A$ for $A > 0$, or $-A < B < -2A$ for $A < 0$. In this case, the effective potential features a local minimum and a maximum, which are found respectively at $x_0 < 0$ and $x_0 > 0$ for $A > 0$, and vice versa for $A < 0$. The extrema – the location of which defines relevant fixed points in the dynamical system (14) – emerge (as per the saddle-center bifurcation mentioned above) close to the location of the potential and nonlinearity steps, i.e., near $x = 0$. The locations $x_{0\pm}$ of the extrema are given by Eq. (16); as an example, using parameter values $V_L = 0$, $V_R = -0.01$, $\alpha_L = 1$ and $\alpha_R = 1.015$, we find that $x_{0+} = 0.66$ ($x_{0-} = -0.66$) for the minimum (maximum).

As the nonlinearity step becomes deeper, the asymptotes (for $x_0 \to \pm\infty$) of $W(x_0)$ become smaller and eventually vanish. For fixed $V_L = 0$ (and $\mu_L = 1$), Eq. (15) shows that this happens for $B = -(3/2)A$; in this case, the potential features a minimum and a maximum in the vicinity of $x_0 = 0$ (see, e.g., upper panel of Fig. 8 below). For $B < -(3/2)A$, the asymptotes of $W(x_0)$ become finite again, and take a positive (negative) value for $x_0 < 0$, and a negative (positive) value for $x_0 > 0$, in the case $A > 0$ ($A < 0$). The form of $W(x_0)$ featuring the extrema in the vicinity of $x_0 = 0$ is preserved in this case too, but as B decreases the extrema eventually disappear, as shown in the insets III and VI of Fig. 1.

D. Solitons at the fixed points of the effective potential

The above analysis poses an interesting question regarding the existence of stationary solitons of Eq. (5) at the extrema of
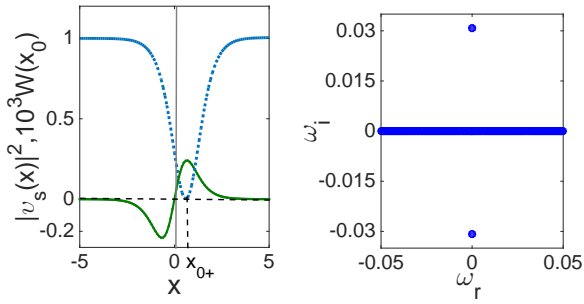
FIG. 2: (Color online) Left panel: density profile of the stationary soliton [dotted (blue) line] at the hyperbolic fixed point $x_{0+} = 0.66$, as found numerically, using the initial guess $v_s(x) = [1 - V(x)]^{1/2}\tanh(x)$ in Eq. (17), for $\alpha_R/\alpha_L = 0.985$, $V_R = 0.01$, $V_L = 0$, $\mu_L = 1$; solid (green) line illustrates the corresponding effective potential $W(x_0)$. Right panel: corresponding spectral plane (ω_r, ω_i) of the corresponding eigenfrequencies, showing a pair of imaginary eigenfrequencies, indicating dynamical instability of the solution.
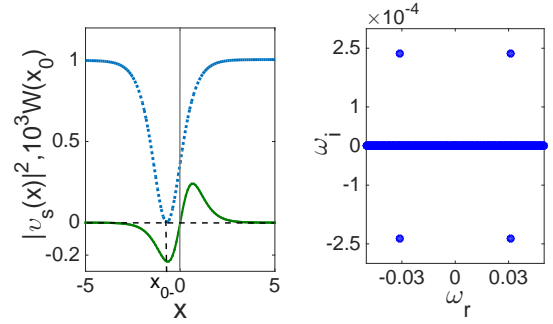
FIG. 3: (Color online) Same as Fig. 2, but for a soliton located at the elliptic fixed point $x_{0-} = -0.66$; this state is found using the initial guess $v_s(x) = [1 - V(x)]^{1/2}\tanh(x + 0.2)$. The spectral plane in the right panel illustrates an oscillatory growth due to the presence of a complex quartet of eigenfrequencies.

the effective potential, associated with the fixed points of the dynamical system (14). To address this question, we use the initial guess $u(x, t) = \exp(-it)v_s(x)$, for a stationary soliton $v_s(x)$, and obtain from Eq. (5) the equation:

$$v_s = -\frac{1}{2}\frac{d^2 v_s}{dx^2} + \frac{\alpha(x)}{\alpha_L}|v_s|^2 v_s + V(x)v_s. \quad (17)$$

Notice that we have assumed without loss of generality a unit frequency solution; the formulation below can be used at will for any other frequency. The above equation is then solved numerically, by means of Newton's method, employing the initial guess:

$$v_s(x) = n^{1/2}(x)\tanh(x - x_0), \quad (18)$$

where

$$n(x) = (1 - V(x))/(\alpha(x)/\alpha_L), \quad (19)$$

is the relevant background density (recall that $n(x) = n_L = 1$ for $x < 0$, and $n(x) = n_R = (1 - V_R)/(\alpha_R/\alpha_L)$ for $x > 0$, as per our normalizations). As shown in the left panel of Fig. 2, employing an initial guess as per Eq. (18), in which the soliton is initially placed at $x_0 = 0$, we find a steady state exactly at the hyperbolic fixed point $x_{0+} = 0.66$, as found from Eq. (16). On the other hand, the left panel of Fig. 3 shows a case where the initial guess in Eq. (18) assumes a soliton placed at $x_0 = -0.2$, which leads to a stationary soliton located exactly at the elliptic fixed point $x_{0-} = -0.66$ predicted by Eq. (16).

It is now relevant to study the stability of these stationary soliton states, performing a Bogoliubov-de Gennes (BdG) analysis [9, 10, 64]. We thus consider small perturbations of $v_s(x)$, and seek solutions of Eq. (5) of the form:

$$u(x, t) = e^{-it}\left[v_s(x) + \delta\left(b(x)e^{-i\omega t} + \bar{c}(x)e^{i\bar{\omega} t}\right)\right], \quad (20)$$

where $(b(x), c(x))$ are eigenfunctions, $\omega = \omega_r + i\omega_i$ are (generally complex) eigenfrequencies, and $\delta \ll 1$. Importantly, the occurrence of a complex eigenfrequency always leads to a dynamic instability; thus, a linearly stable configuration is tantamount to $\omega_i = 0$ (i.e., all eigenfrequencies are real). It should also be noted that, due to the Hamiltonian nature of the system, if ω is an eigenfrequency of the Bogoliubov spectrum, so are $-\omega$, $\bar{\omega}$ and $-\bar{\omega}$.

Substituting Eq. (20) into Eq. (5), and linearizing with respect to δ, we derive the following BdG equations:

$$\left[\hat{H} - 1 + 2\frac{\alpha(x)}{\alpha_L}v_s^2\right]b + \frac{\alpha(x)}{\alpha_L}v_s^2 c = \omega b, \quad (21)$$

$$\left[\hat{H} - 1 + 2\frac{\alpha(x)}{\alpha_L}v_s^2\right]c + \frac{\alpha(x)}{\alpha_L}v_s^2 b = -\omega c, \quad (22)$$

where $\hat{H} = -(1/2)\partial_x^2 + V(x)$ is the single particle operator. This eigenvalue problem is then solved numerically. Examples of the stationary dark solitons at the fixed points $x_{0\pm}$ associated with the effective potential W, as well as their corresponding BdG spectra, are shown in Figs. 2 and 3. It is observed that the solitons are dynamically unstable, as seen by the presence of eigenfrequencies with nonzero imaginary part in the spectra, although the mechanisms of instability are distinctly different between the two cases in Figs. 2 and 3. It should also be noted that for each eigenfunction pair (b, c), an important quantity to be used below is the so-called signature $K = \int_{-\infty}^{\infty}|b|^2 - |c|^2 dx$, as is discussed in detail, e.g., in [9, 69]. The presence of eigenvalues of negative signature illustrates the excited state of the configuration of interest (as is the case, e.g., with the dark solitons considered herein) and a key feature is that the collision of two eigenvalues of different signature will lead to an instability associated with an eigenvalue quartet $(\omega, -\omega, \bar{\omega}, -\bar{\omega})$.

To better understand these instabilities, and also provide an analytical estimate for the relevant eigenfrequencies, we may follow the analysis of Ref. [66]; see also Ref. [67] for application of this theory to the case of a periodic, piecewise-constant scattering length setting. According to these works, solitons persist in the presence of the perturbation $P(v)$ of Eq. (8) (of
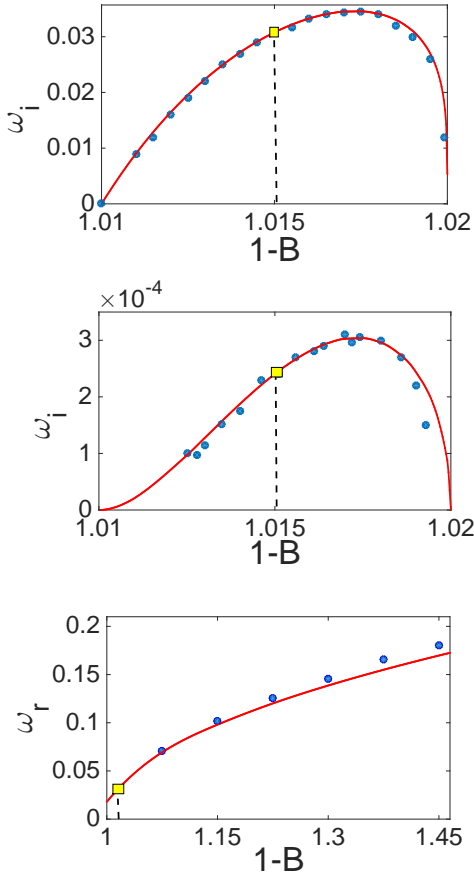
FIG. 4: (Color online) Top panel: the imaginary part of the eigenfrequency, ω_i, as a function of $1 - B$ (with $B < 0$), for a soliton located at the hyperbolic fixed point, $x = x_{0+}$. Middle and bottom panels show the dependence of imaginary and real parts, ω_i and ω_r, of the eigenfrequency on $1 - B$, for a soliton located at the elliptic fixed point, $x = x_{0-}$, i.e., the case that leads to an eigenfrequency quartet. Solid (red) curves correspond to the analytical prediction [cf. Eqs. (25) and (26)], (blue) circles depict numerical results, while (yellow) squares depict eigenfrequency values corresponding to the cases shown in Figs. 2 and 3. For the top and middle panels $A = 0.01$, while for the bottom panel $A = -(2/3)B$; in all cases, $\mu_L = 1$.

strength A, $B \sim \epsilon$) provided that the Melnikov function

$$M'(x_0) = \int_{-\infty}^{+\infty} \frac{\partial U}{\partial x} \left(1 - \tanh^2(x - x_0) \right) dx = 0, \quad (23)$$

vanishes, i.e., the equation $M'(x_0) = 0$ possesses at least one root, say $\tilde{x}_0$. This result can be obtained by starting from the steady state equation

$$\frac{1}{2} \frac{\partial^2 v}{\partial x^2} - \left(|v|^2 - 1 \right) v = P(v) \equiv U(v(x))v. \quad (24)$$

Upon multiplication by $\partial v/\partial x$, the left hand side yields $\int_{-\infty}^{\infty} \frac{dE}{dx} dx$ where $E = \frac{1}{2} \left(\frac{\partial v}{\partial x} \right)^2 + \frac{1}{2}(v^2 - 1)^2$, while the right hand side will yield, upon integration by parts, the solvability

condition (23). In our case, we find that this equation has exactly two zeros, namely the fixed points $x_{0\pm}$, i.e., $\tilde{x}_0 = x_{0\pm}$.

Then, the stability of the dark soliton solutions at $x_{0\pm}$ depends on the sign of the derivative of the Melnikov function in Eq. (23), evaluated at $\tilde{x}_0 = x_{0\pm}$. Generally speaking, an instability occurs, with one imaginary eigenfrequency pair for $\epsilon M''(\tilde{x}_0) < 0$, and with exactly one complex eigenfrequency quartet for $\epsilon M''(\tilde{x}_0) > 0$. The instability is dictated by the translational eigenvalue of the BdG Eqs. (21)-(22), which bifurcates from the origin as soon as the perturbation is present. I.e., the translational mode with eigenfunction proportional to the derivative of the wave is neutral (associated with $\omega = 0$) in the case of a homogeneous domain, but acquires a non-vanishing ω, in our case of a spatially inhomogeneous domain since the symmetry of translational invariance is broken. For $\epsilon M''(\tilde{x}_0) < 0$, the relevant eigenfrequency pair moves along the imaginary axis, leading to an immediate instability associated with exponential growth of a perturbation along the relevant eigendirection. On the other hand, for $\epsilon M''(\tilde{x}_0) > 0$, the eigenfrequency moves along the real axis but becomes a negative signature mode (due to the excited state nature of the dark soliton). Then, upon collision (resonance) with eigenfrequencies of modes of opposite signature than that of the translation mode, it gives rise to a complex eigenfrequency quartet, signaling the presence of an oscillatory instability.

The eigenfrequencies can be determined by a quadratic characteristic equation which takes the form [66],

$$\lambda^2 + \frac{1}{4} M''(\tilde{x}_0) \left(1 - \frac{\lambda}{2} \right) = \mathcal{O}(\epsilon^2), \quad (25)$$

where eigenvalues λ are related to eigenfrequencies ω through $\lambda^2 = -\omega^2$. The derivation of the latter formula Eq. (25) is rather elaborate and hence is not expanded upon here; the interested reader is directed to Theorem 4.11 and associated discussion of [66] for a systematic derivation. Since, in our case, the zeros of $M'(x_0)$ are the two fixed points $x_{0\pm}$ as mentioned above, we may evaluate $M''(\tilde{x}_0)$ at $\tilde{x}_0 = x_{0\pm}$ explicitly, and obtain:

$$M''(x_{0\pm}) = - \ 2\text{sech}^2(x_{0\pm}) \tanh(x_{0\pm})$$
$$\times \ \left[A + B \tanh^2(x_{0\pm}) \right]. \quad (26)$$

To this end, substituting the result of Eq. (26) into Eq. (25), yields an analytical prediction for the magnitudes of the relevant eigenfrequencies, for the cases of solitons located at the hyperbolic or the elliptic fixed points.

Figure 4 shows pertinent analytical results [depicted by (red) solid curves], which are compared with corresponding numerical results [depicted by (blue) points]. In particular, the top panel of the figure illustrates the dependence of the imaginary part of the eigenfrequency ω_i on the parameter $1 - B$ (with $B < 0$), for a soliton located at the hyperbolic fixed point, $x = x_{0+}$; this case is associated with the scenario $M''(x_0) < 0$. The middle and bottom panels of the figure show the dependence of ω_i and ω_r on $1 - B$, but for a soliton located at the elliptic fixed point, $x = x_{0-}$; in this case, $M''(x_0) > 0$, corresponding to an oscillatory instability as mentioned above. It is readily observed that the agreement between the theoretical prediction of Eqs. (25) and (26) and the

numerical result is very good; especially, for values of $1 - B$ close to unity, i.e., in the case $|B| \lesssim 0.15$ where perturbation theory is more accurate, the agreement is excellent.

We should also remark here that a similarly good agreement between analytical and numerical results was also found (results not shown here) upon using as an independent parameter the strength of the potential step ($\sim A$), instead of the strength of the nonlinearity step ($\sim B$), as in the case of Fig. 4.

E. The instabilities in the PDE and ODE pictures

As mentioned above, one of the purposes of this work is to investigate possible trapping (or quasi-trapping) of solitons in the vicinity of the potential and nonlinearity steps. Candidate locations for such a trapping are the ones of the elliptic and hyperbolic fixed points (where stationary solitons do exist, as shown in the previous subsection). However, both fixed points were found to be unstable in the BdG analysis. It is, therefore, relevant to discuss in more detail the nature and significance of these instabilities in the PDE and ODE pictures.

First, in the case of the hyperbolic fixed point, the existence of a single pair of unstable (real) BdG eigenvalues is naturally expected and consistent with our analytical approximation and the ODE picture: indeed, these real eigenvalues are in fact a manifestation of the unstable nature of the fixed point, with the relevant eigenfrequency being related to the harmonic approximation of the "expulsive" peak (maximum) of the effective potential.

On the other hand, the existence of the elliptic fixed point suggests that, this one, could potentially trap solitons reliably for a long time. Nevertheless, solitons at the elliptic fixed point are subject to an oscillatory instability, as predicted by the BdG analysis. This fact needs to further be investigated, both in terms of the connection with the equivalent particle approach, and of the consequences to the soliton dynamics.

For this purpose, first we use the BdG analysis to determine the eigenfunctions $b(x)$ and $c(x)$ of Eqs. (21)-(22), corresponding to the complex eigenfrequency quartet. The result is shown in the left panel of Fig. 5; as is observed, these eigenfunctions are strongly localized within the dark soliton's notch. Importantly, an excitation of the stationary soliton located at the elliptic fixed point $x_{0-} = -0.66$ by this eigenmode, results in a *displacement* $(\Delta x_0) = -0.1$ of the soliton from x_{0-}; this is illustrated in the right panel of Fig. 5, where the unperturbed [solid (black) line] and the perturbed [dashed (red) line] for the soliton densities are shown.

Nevertheless, such an excitation of the soliton along this eigendirection, can not lead the soliton to a stable periodic orbit around the fixed point (as the ODE picture would suggest): this is due to the fact that this eigendirection is unstable, characterized by a complex eigenfrequency. Intuitively, this represents a resonance between the oscillation of the dark soliton and one of the extended background modes (continuous spectrum) of the PDE, leading to energy exchange between the soliton and the background. Given the absence of the latter modes in the ODE formulation, it is not surprising that this feature is not captured in the ODE picture. This coupling to
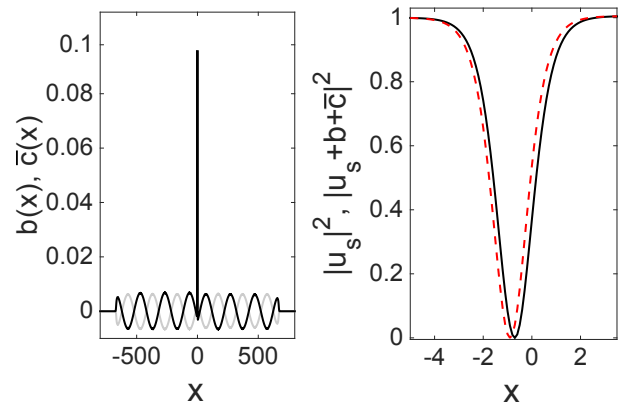

FIG. 5: (Color online) Left panel: eigenfunctions $b(x)$ (black line) and $c(x)$ (gray line) of Eqs. (21)-(22), corresponding to the complex eigenfrequency quartet (associated to the elliptic fixed point). Right panel: solid (black) line shows the density of the stationary dark soliton at the elliptic fixed point $x_{0-} = -0.66$; dashed (red) line shows the density of the dark soliton when excited by this mode, which results in a displacement from x_{0-} by $(\Delta x_0) = -0.1$. Parameter values are as in Fig. 3.

radiation modes causes the dark soliton to increase its speed. Hence, the soliton is expected to perform oscillations of growing amplitude around the elliptic fixed point, with a frequency and growth rate given by the real and imaginary parts of the eigenfrequency, respectively. This suggests that the soliton may eventually escape from the vicinity of the elliptic fixed point. In other words, although the ODE picture suggests that the fixed point x_{0-} is an elliptic one, the BdG analysis [and, consequently, the partial differential equation (PDE) picture], suggests that the fixed point is, in fact, an *unstable spiral*.

The above arguments are supported by direct simulations at the level of the GP Eq. (5). Indeed, in the top panel of Fig. 6, shown is a contour plot depicting the evolution of a soliton density, initially located at the elliptic fixed point, which is perturbed along the unstable eigendirection. In other words, to numerically integrate the GP Eq. (5), we use the initial condition $u(0) = u_s + b + \bar{c}$, where u_s is the dark soliton at the elliptic fixed point – cf. also the right panel of Fig. 5 (parameter values are identical to those of Fig. 3). It is readily observed that the soliton, having been displaced from the location of the elliptic fixed point, performs small-amplitude oscillations around it. At an "early" stage of the evolution – cf. inset of the top panel of Fig. 6 – the soliton oscillations are well approximated by the ODE Eq. (14): the latter, for an initial condition $x_0(0) = x_{0-} + (\Delta x_0)$, yields an oscillation frequency $\omega_{osc} \approx 0.03$, which is almost identical to the real part ω_r of the eigenfrequency of the unstable eigenmode, namely $\omega = \omega_r + i\omega_i = 0.031 + i0.00023$. This is illustrated in the inset of the top panel of Fig. 6, where the ODE result is depicted by the thin solid (white) line. Nevertheless, the oscillations are, in fact, of growing amplitude – due to the nonzero imaginary part of the eigenfrequency; this becomes evident at later times and, as a result, the soliton finally escapes from the vicinity of the elliptic fixed point.
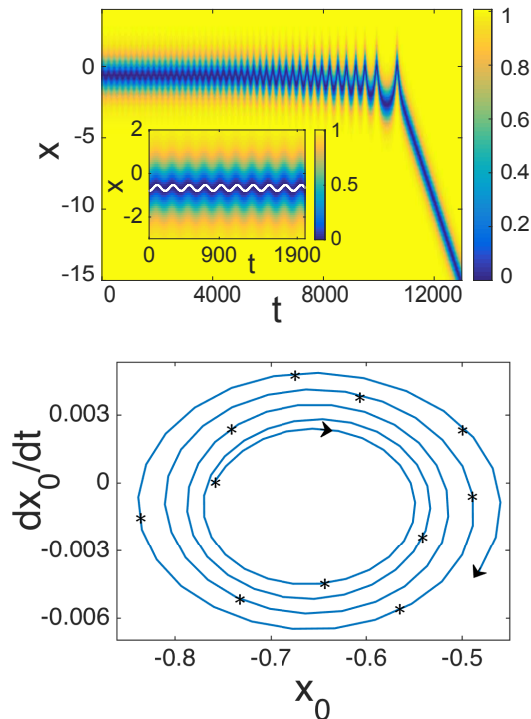
FIG. 6: (Color online) Top panel: contour plot showing the evolution of the density of a dark soliton, which is initially displaced by $(\Delta x_0) = -0.1$ from the elliptic fixed point $x_{0-} = -0.66$ along the unstable eigendirection (cf. right panel of Fig. 5); the initial soliton velocity is zero. At an early stage of the evolution, the soliton oscillation frequency as found by the ODE Eq. (14) is almost identical to the real part of the complex eigenfrequency $\omega = \omega_r + i\omega_i$, namely $\omega_{\rm osc} = \omega_r = 0.031$ (see inset). The amplitude of oscillations is growing, due to the presence of the imaginary part of ω, namely $\omega_i = 0.00023$. Thick solid (blue) lines in the color coded carpet plot show PDE results, while thin solid (white) line in the inset depicts the ODE result. Bottom panel: the corresponding phase plane, highlighting the unstable spiral dynamics, taken from the PDEs (solid curve) and from Eq. (27) (stars), for time up to $t = 6000$.

The bottom panel of Fig. 6 illustrates the fact that the fixed point of the ODE Eq. (14) is actually an unstable spiral in the PDE picture: indeed, this panel illustrates the soliton trajectory, as obtained from the PDE simulation, in the phase plane $(dx_0/dt,\, x_0)$ for a time up to $t = 6000$ – cf. solid (blue) line. This soliton trajectory can be well approximated analytically – cf. stars in bottom panel of Fig. 6 – upon using the following expression that describes the spiraling-outwards motion of the soliton center:

$$x_0(t) = x_{0-} + (\Delta x_0)\exp(\omega_i t)\cos(\omega_r t), \qquad (27)$$

where $x_{0-} = -0.66$ is the location of the elliptic fixed point as found by the ODE, $(\Delta x_0) = -0.1$ is the displacement of the soliton due to the addition of the unstable eigenmode (cf. dashed (red) line in the right panel of Fig. 5), while $\omega_r = 0.031$ and $\omega_i = 0.00023$ are the real and imaginary parts of the eigenfrequency, as mentioned above. Obviously, the initial soliton position is $x_0(0) = x_{0-} + (\Delta x_0) = -0.76$, while the

intial soliton velocity is $dx_0(0)/dt = 0$ (cf. the relevant star in the figure, where the unstable spiral starts). Clearly, the approximation, up to the time $t = 6000$, is very good.

Concluding this section, it is evident that trapping of the soliton at the elliptic fixed point is not possible. For this reason, below, attention will be paid to possible (quasi-)trapping of the soliton at the hyperbolic fixed point (when present) of the effective potential. Our effort will rely on on preparing the initial condition at the stable manifold, a process, however, that suffers from a well-known sensitivity on the initial conditions. In any case, in the context of optics, such a soliton trapping effect could be viewed as a formation of a surface dark soliton at the interfaces between optical media exhibiting different linear refractive indices and different defocusing Kerr nonlinearities (or atomic media bearing different linear potential and interparticle interaction properties at the two sides of the interface).

III. DARK SOLITON DYNAMICS

We now turn our attention to the dynamics of dark solitons near the potential and nonlinearity steps. We will use, as a guideline, the analytical results presented in the previous section, and particularly the form of the effective potential. Our aim is to study the scattering of a dark soliton, initially located in the region $x < 0$ and moving to the right, at the potential and nonlinearity steps (similar considerations, for a soliton located in the region $x > 0$ and moving to the left, are straightforward, hence only limited examples of the latter type will be presented). We will consider the scattering process in the presence of:

(a) a single potential step,

(b) a potential and nonlinearity step, and

(c) rectangular barriers, formed by two potential and nonlinearity steps.

In the simulations below, we use a high accuracy spectral method to numerically integrate Eq. (5), and – unless stated otherwise – we fix the parameter values as follows: $V_0 = 10$ and $w = 250$ (for the box potential), $V_{\rm L} = 0$ and $V_{\rm R} = \pm 0.01$ for the potential step, as well as $\alpha_{\rm L} = 1$ and $\alpha_{\rm R} \in [0.9, 1.1]$ for the nonlinearity step. Nevertheless, our theoretical approach is general (and will be kept as such in the exposition that follows in this section).

A. A single potential step

Our first scattering "experiment" refers to the case of a potential step only, corresponding to $A > 0$ and $B = 0$ (cf. inset I in Fig. 1). In this case, the effective potential is similar to the $\tanh$ function, while the associated phase-plane is shown in the middle panel of the same figure. Clearly, according to the particle picture for the soliton of the previous
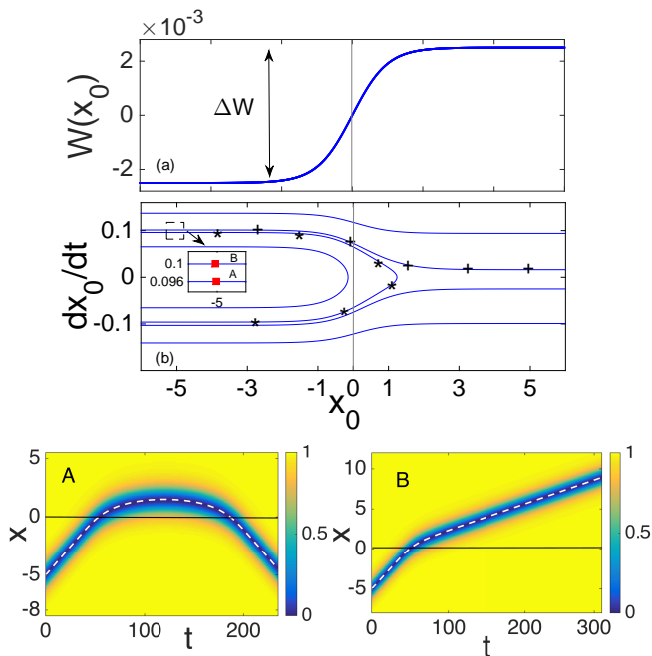
FIG. 7: (Color online) The case of a single potential step, $A = 0.01$ and $B = 0$, corresponding to $V_L = 0$, $V_R = 0.01$, $\alpha_R = \alpha_L$, and $\mu_L = 1$. Top panel (a): effective potential $W(x_0)$; shown also is the potential difference $\Delta W = W(+\infty) - W(-\infty) = 4.99 \times 10^{-3}$. Middle panel (b): corresponding phase plane; inset shows the initial conditions [(red) squares A and B] for the trajectories corresponding to reflection or transmission, while stars and pluses depict respective PDE results. Bottom panels: contour plots showing the evolution of the dark soliton density for the initial conditions depicted in the middle panel, i.e., $x_0 = -5$ and $\phi = 9.6 \times 10^{-2}$ (left), or $\phi = 0.1$ (right); note that, here, $\phi_c = 0.099$. Thick (blue) solid curves in the color coded carpet plot show PDE results, while dashed (white) curves depict ODE results.

section, a dark soliton incident from the left towards the potential step can either be reflected or transmitted: if the soliton has a velocity $v = dx_0/dt$, and thus a kinetic energy

$$K = \frac{1}{2}v^2 = \frac{1}{2}\sin^2\phi \approx \frac{1}{2}\phi^2, \tag{28}$$

smaller (greater) than the effective potential step $\Delta W = W(+\infty) - W(-\infty)$, as shown in the top panel of Fig. 7, then it will be reflected (transmitted). Notice the approximation ($\sin\phi \approx \phi$) here which is applicable for low speeds/kinetic energies. This consideration leads to $\phi < \phi_c$ or $\phi > \phi_c$ for reflection or transmission, where the critical value ϕ_c of the soliton phase angle is given by:

$$\phi_c = \sqrt{2\Delta W}. \tag{29}$$

In the numerical simulations we found that the threshold between the two cases is quite sharp and is accurately predicted by Eq. (29). Indeed, consider the scenario shown in Fig. 7, corresponding to parameter values $V_L = 0$, $V_R = 0.01$, $\alpha_R = \alpha_L$ and $\mu_L = 1$. In this case, we find that $\Delta W = 4.99 \times 10^{-3}$, which leads to the critical value (for reflection/transmission)

of the soliton phase angle $\phi_c = 9.99 \times 10^{-2}$. Then, for a soliton initially placed at $x_0 = -5$, and for initial velocities corresponding to phase angles $\phi = 9.6 \times 10^{-2}$ or $\phi = 0.1$, we observe reflection or transmission, respectively. The corresponding soliton trajectories are depicted both in the phase plane $(x_0, dx_0/dt)$ in the middle panel of Fig. 7 and in the space-time contour plots showing the evolution of the soliton density in the bottom panels of the same figure (see trajectories A and B for reflection and transmission, respectively). Note that stars and pluses in the middle panel correspond to results obtained by direct numerical integration of the partial differential equation (PDE), Eq. (5), while the (white) dashed curves in the bottom panels depict results obtained by the ODE, Eq. (14). Obviously, the agreement between theoretical predictions and numerical results is very good.

Here we should recall that in the case where the nonlinearity step is also present ($B \neq 0$), and when $B > -A$ (for $A > 0$) or $B < -A$ (for $A < 0$), the form of the effective potential is similar to the one shown in the top panel of Fig. 7. In such cases, corresponding results (not shown here) are qualitatively similar to the ones presented above.

B. A potential and a nonlinearity step

Next, we study the case where both a potential and a nonlinearity step are present (i.e., $A, B \neq 0$), and there exist fixed points in the effective particle picture. One such case that we consider in more detail below is the one corresponding to $A = 0.01$ and $B = -0.015$ (respective parameter values are $V_L = 0$, $V_R = 0.01$, $\alpha_R/\alpha_L = 0.985$, and $\mu_L = 1$). Note that for this choice the effective potential asymptotically vanishes, as shown in the top panel of Fig. 8; nevertheless, results qualitatively similar to the ones that we present below can also be obtained for nonvanishing asymptotics of $W(x_0)$.

The form of the effective potential now suggests the existence of an elliptic and a hyperbolic fixed point, located at $x_0 \approx \mp 0.65$ respectively. In this case too, one can identify an energy threshold ΔW, now defined as $\Delta W = W(x_{0+}) - W(-\infty) = W(x_{0+})$, needed to be overcome by the soliton kinetic energy in order for the soliton to be transmitted (otherwise, i.e., for $K < \Delta W$, the soliton is reflected). Using the above parameter values, we find that $\Delta W = 2.4 \times 10^{-4}$ and, hence, according to Eq. (29), the critical phase angle for transmission/reflection is $\phi_c \approx 0.022$. In the simulations, we considered a soliton with initial position and phase angle $x_0 = -5$ and $\phi = 0.034 > \phi_c$, respectively (cf. point A in the phase plane shown in the second panel of Fig. 8), and found that, indeed, the soliton is transmitted through the effective potential barrier of strength ΔW. The respective trajectory (starting from point A) is shown in the second panel of Fig. 8. Asterisks along this trajectory, as well as contour plot A in the same figure, show PDE results obtained from direct numerical integration of Eq. (5); as in the case of Fig. 7, the dashed (white) line corresponds to the ODE result.

To study the possibility of soliton trapping, we have also used an initial condition at the stable branch, incoming towards the hyperbolic fixed point, namely $x_0 = -5$ and
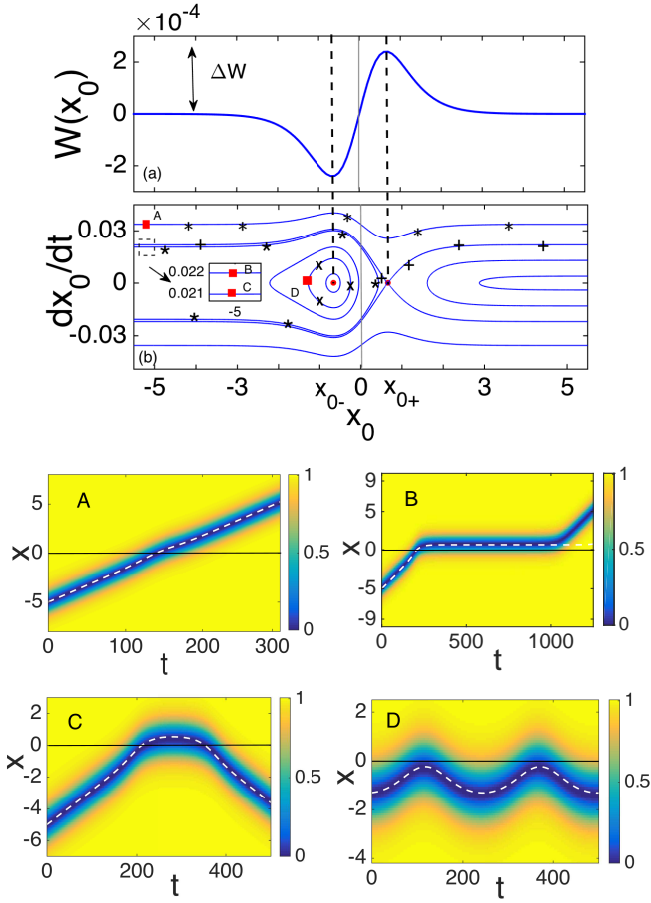
FIG. 8: (Color online) Similar to Fig. 7, but for a potential and a nonlinearity step, with $B = -(3/2)A$, i.e., $A = 0.01$ and $B = -0.015$, corresponding to $V_L = 0$, $V_R = 0.01$, $\alpha_R/\alpha_L = 0.985$, and $\mu_L = 1$. Top and bottom panels show the effective potential $W(x_0)$ and the associated phase plane, respectively; now, an elliptic and a hyperbolic fixed point exist at $x_0 \approx \pm 0.65$ (cf. vertical dashed lines). In the phase plane, initial conditions – marked with (red) squares – at points A ($x_0 = -5$, $\phi = 0.034$), B ($x_0 = -5$, $\phi = 0.022$), C ($x_0 = -5$, $\phi = 0.021$) and D ($x_0 = -1.3$, $\phi = 0.002$) lead to soliton transmission, quasi-trapping, reflection, and oscillations around the elliptic fixed point, respectively; asterisks, pluses, crosses and stars depict PDE results. The four bottom respective contour plots show the evolution of the soliton density; again, dashed (white) curves depict ODE results.

$\phi = \phi_c \approx 0.022$ (point B in the second panel of Fig. 8). In this case, the soliton reaches at the location of the hyperbolic fixed point (cf. incoming branch, marked with pluses) and appears to be trapped at the saddle; however, this trapping occurs only for a finite time (for $t \approx 600$). At the PDE level, this can be understood by the the fact that such a configuration (i.e., a stationary dark soliton located at the hyperbolic fixed point) is unstable, as per the analysis of Sec. II.D. Then, the soliton escapes and moves to the region of $x > 0$, following the trajectory marked with pluses for $x > x_{0+}$ (here, the pluses depict the PDE results). The corresponding contour plot B, in the third panel of Fig. 8, shows the evolution of the dark soliton density. Note that, in this case, the result obtained by the ODE

[cf. dashed (white) line] is only accurate up to the escape time, as small perturbations within the infinite-dimensional system destroy the delicate balance of the unstable fixed point.

For the same form of the effective potential, we have also used initial conditions that lead to soliton reflection. In particular, we have again used $x_0 = -5$ and $\phi = 0.021 < \phi_c$, as well as an initial soliton location closer to the potential and nonlinearity step, namely $x_0 = -1.3$, and $\phi = 0.002$. These initial conditions are respectively indicated by the (red) squares C and D in the second panel of Fig. 8. Relevant trajectories in the phase plane, as well as respective PDE results (cf. stars and crosses), can also be found in the same panel, while contour plots C and D in the bottom panel of Fig. 8 show the evolution of the soliton densities. It can readily be observed that for the slightly subcritical value of the phase angle ($\phi = 0.021$), the soliton is again quasi-trapped at the hyperbolic fixed point, but for a significantly smaller time (for $t \approx 150$). On the other hand, when the soliton is initially located closer to the steps and has a sufficiently small initial velocity, it performs oscillations, following the periodic orbit shown in the second panel of Fig. 8.

In all the above cases, we find a very good agreement between the analytical predictions and the numerical results. Similar agreement was also found for other forms of the effective potential, as shown, e.g., in the example of Fig. 9 (see also inset III of Fig. 1). For this form of $W(x_0)$, parameters A and B are $A = 0.01$ and $B = -0.017$ (for $V_L = 0$, $V_R = 0.01$, $\alpha_R/\alpha_L = 0.983$, and $\mu_L = 1$), while there exist again an elliptic and a hyperbolic fixed point, at $x_{0\pm} = \pm 0.44$ respectively. In such a situation, if a soliton moves from the left towards the potential and nonlinearity steps, and is placed sufficiently far from (close to) them – cf. initial condition at point A (point B) – then it will be transmitted (perform oscillations around x_{0-}). On the other hand, if a soliton is initially placed at some $x_0 > x_{0+}$ and moves to the left towards the potential and nonlinearity steps, it faces an effective barrier ΔW (cf. top panel of Fig. 9), now defined as $\Delta W = W(x_{0+}) - W(+\infty)$. In this case too, choosing an initial condition corresponding to the stable branch, incoming towards x_{0+}, i.e., for the critical phase angle $\phi_c \approx 0.03$, it is possible and achieve quasi-trapping of the soliton for a finite time, of the order of $t \approx 600$. As such a situation was already discussed above (cf. panel B of Fig. 8), here we present results pertaining to the slightly supercritical case, namely $\phi = 0.031 > \phi_c$; cf. (red) squares C in the second panel, and the corresponding contour plot in the bottom panel of Fig. 9. It is readily observed that the soliton is initially transmitted through the interface; however, it then follows a trajectory surrounding the homoclinic orbit (see the orbit marked with plus symbols, which depicts the PDE results, in the second panel of Fig. 9), and is eventually reflected. Note that in the subcritical case of $\phi = 0.029 < \phi_c$ (see point D in the second panel of Fig. 9), the soliton reaches x_{0+}, stays there for a time $t \approx 180$, and eventually is reflected back following the trajectory marked with asterisks, as shown in the second panel of Fig. 9. Again, in all cases pertaining to this form of $W(x_0)$, the agreement between the analytical predictions and the numerical results is very good.
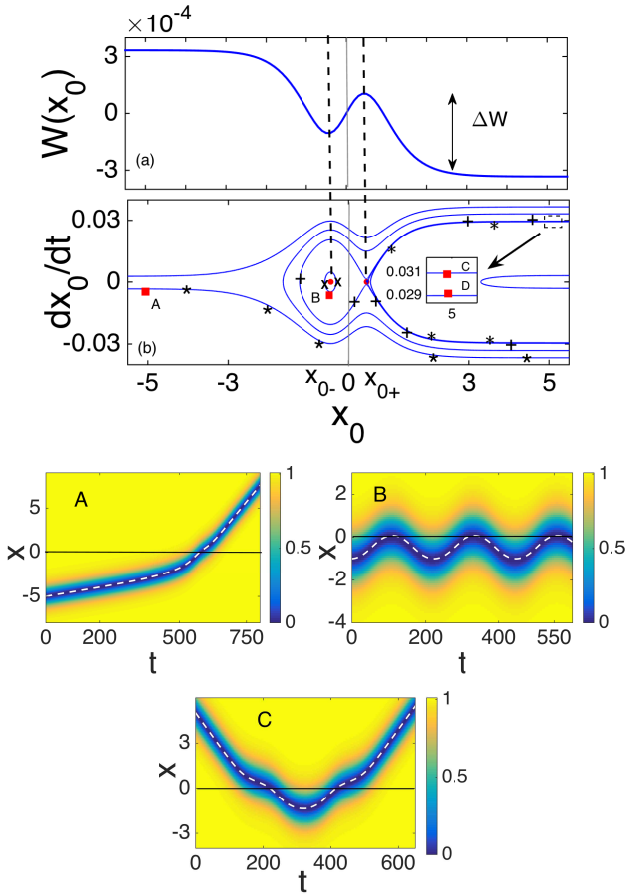
FIG. 9: (Color online) Similar to Fig. 8, for a potential and a nonlinearity step, but now for $A = 0.01$ and $B = -0.017$, corresponding to $V_L = 0$, $V_R = 0.01$, $\alpha_R/\alpha_L = 0.983$, and $\mu_L = 1$. The form of $W(x_0)$ (top panel) suggests the existence of an elliptic and a hyperbolic fixed point, at $x_{0\pm} = \pm 0.44$ (vertical dashed lines). In the phase plane (second panel) shown are initial conditions, for a soliton moving to the right, at points A ($x_0 = -5$, $\phi = 0.005$) and B ($x_0 = -1$, $\phi = 0.001$), as well as for a soliton moving to the left, at points C ($x_0 = 5$, $\phi = 0.031 > \phi_c \approx 0.030$) and D ($x_0 = 5$, $\phi = 0.029 < \phi_c$); in the relevant trajectories, stars, crosses, pluses, and asterisks, respectively, denote PDE results. Corresponding contour plots A, B, and C for the soliton density are shown in the bottom panels, with the dashed (white) lines depicting ODE results.

C. Rectangular barriers

Our analytical approximation can straightforwardly be extended to the case of multiple potential and nonlinearity steps. Here, we will present results for such a case, where two steps, located at $x = -L$ and $x = L$, are combined so as to form rectangular barriers, in both the linear potential and the nonlinearity of the system. In particular, we consider the follow-

ing profiles for the potential and the scattering length:

$$V(x) = V_b(x) + \begin{cases} V_R, & |x| > L \\ V_L, & |x| < L \end{cases}, \qquad (30)$$

$$\alpha(x) = \begin{cases} \alpha_R, & |x| > L \\ \alpha_L, & |x| < L \end{cases}. \qquad (31)$$

In such a situation, the effective potential can be found following the lines of the analysis presented in Sec. II.B: taking into regard that the perturbation $P(v)$ in Eq. (7) has now the form:

$$P(v) = \left(A + B|v|^2 \right) v \left[\mathcal{H}(x+L) - \mathcal{H}(x-L) \right], \quad (32)$$

it is straightforward to find that the relevant effective potential is given by:

$$\begin{aligned} W(x_0) &= \frac{1}{8} \left(2A + B \right) \left[\tanh(L - x_0) + \tanh(L + x_0) \right] \\ &+ \frac{1}{24} B [\tanh^3(L - x_0) + \tanh^3(L + x_0)]. \quad (33) \end{aligned}$$

Typically, i.e., for sufficiently large arbitrary values of L, the effective potential is as shown in the top panel of Fig. 10; in this example, we used $L = 5$, while $A = 0.01$ and $B = -0.015$. It is readily observed that, in this case, the effective potential takes the form of a superposition of the ones shown in Fig. 8, which are now located at ± 5. The associated phase plane is shown in the middle panel of Fig. 10; shown also is an initial condition [(red) square point A] corresponding to soliton oscillations around the elliptic fixed point at the origin. The corresponding soliton trajectory is depicted both in the phase plane in the middle panel of Fig. 10 and in the space-time contour plot showing the evolution of the soliton density in the bottom panel of the same figure. Note that quasi-trapping of the soliton is also possible in this case: indeed, we have found that starting from the stable branch, at $x_0 = -8.6$ and $\phi = 2.2 \times 10^{-2}$ (point A in the middle panel of Fig. 10), the soliton is trapped at the hyperbolic fixed point at -4.34 for a time $t \approx 600$, and finally it is reflected back (see trajectory marked with stars); the soliton trajectory in the space-time contour plot is qualitatively similar to the one shown in the bottom left panel of Fig. 7 (result not shown here). Once again, agreement between theoretical predictions and numerical results for this setting is very good as well.

An interesting situation occurs as L decreases. To better illustrate what happens in this case, and also to make connections with earlier work [12], we consider the simpler case of $B = 0$ (i.e., the nonlinearity step is absent). Then, assuming that $A = b/(2L)$ (with b being an arbitrary small parameter), and in the limit of $L \to 0$, the potential step takes the form of a delta-like impurity of strength b. In this case, the effective potential of Eq. (33) is reduced to the form $W(x_0) = (b/4)\text{sech}^2(x_0)$. This result recovers the one reported in Ref. [12] (see also Refs. [8, 13]), where the interaction of dark solitons with localized impurities was studied; cf. Eq. (16) of that work, but in the absence of the trapping potential U_{tr}.
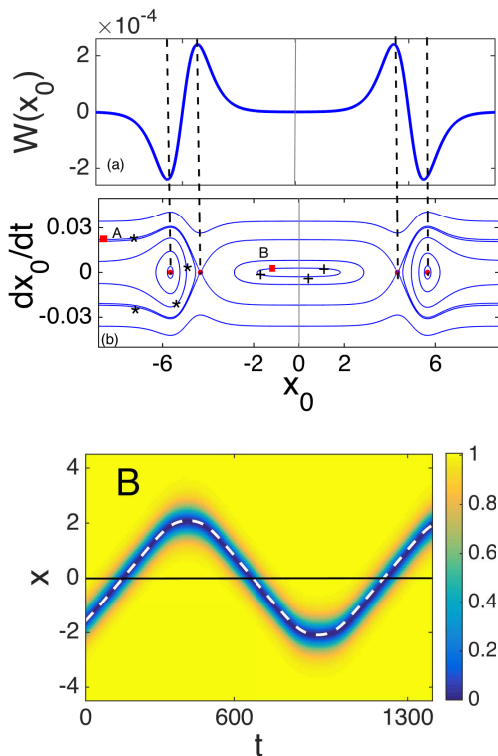
FIG. 10: (Color online) The case of two potential and nonlinearity steps forming respective rectangular barriers, for $L = 5$, $A = 0.01$ and $B = -0.015$, corresponding to $V_L = 0$, $V_R = 0.01$, $\alpha_R/\alpha_L = 0.985$, $\mu_L = 1$. Top panel (a): the effective potential $W(x_0)$ – cf. Eq. (33); dashed lines depict the elliptic fixed points at the origin and at ± 5.66, as well as a pair of hyperbolic fixed points at ± 4.34. Middle panel (b): the associated phase plane; (red) squares A and B depict initial conditions corresponding to quasi-trapping ($x_0 = -8.6$ and $\phi = 2.2 \times 10^{-3}$) or oscillations ($x_0 = -3$ and $\phi = 3 \times 10^{-3}$), while stars and pluses depict respective PDE results. Bottom panel: contour plot showing the evolution of the dark soliton density for the initial condition B depicted in the middle panel; as before, dashed (white) line depicts ODE results.

In the same limiting case of small L, and for $B \neq 0$, the effective potential has typically the form shown in the top panel of Fig. 11; here, we use $L = 0.1$, while $A = 0.1$ and $B = -0.13$, corresponding to $a_R/a_L = 0.87$, $V_R = 0.1$ and $\mu_L = 1$. Comparing this form of $W(x_0)$ with the one shown in Fig. 10, it becomes clear that as $L \to 0$, the individual parts of the effective potential of Fig. 10 pertaining to the two potential/nonlinearity steps move towards the origin. There, they merge at the location of the "central" elliptic fixed point, which becomes unstable through a pitchfork bifurcation. As a result of this process, an unstable (hyperbolic) fixed point emerges at the origin, while the "outer" pair of the elliptic fixed points (cf. Fig. 10) also drift towards the origin – in this case, they are located at ± 1.38.

In the bottom panel of Fig. 11, shown also is the phase plane associated to the effective potential of the top panel. As in the cases studied in the previous sections, we may investigate possible quasi-trapping of the soliton, using an initial
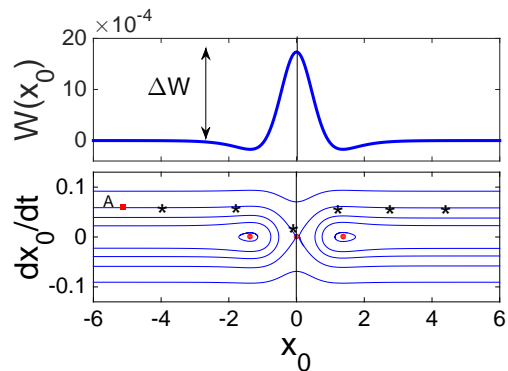

FIG. 11: (Color online) The case of two potential and nonlinearity steps forming respective rectangular barriers, for $L = 0.1$, $A = 0.1$ and $B = -0.13$, corresponding to $a_R/a_L = 0.87$, $V_R = 0.1$ and $\mu_L = 1$. Top panel: the effective potential $W(x_0)$; in this case, there exist a hyperbolic fixed point at the origin and a pair of elliptic fixed points at ± 1.38. Bottom panel: the associated phase plane; (red) square A depicts an initial condition ($x_0 = -5$ and $\phi = 5.8 \times 10^{-2}$) corresponding to quasi-trapping of the soliton, while stars depict respective PDE results.

condition at the stable branch, incoming towards the hyperbolic fixed point at the origin. Indeed, choosing $x_0 = -5$ and $\phi = \phi_c = 5.8 \times 10^{-2}$ (point A, for which the corresponding effective barrier is $\Delta W = 1.7 \times 10^{-3}$), we find the following: the soliton arrives at the origin, stays there for a time $t \approx 600$, and then it is transmitted through the region $x > 0$. The corresponding trajectory found at the PDE level is depicted by stars in the bottom panel of Fig. 11. Notice, again, the fairly good agreement between numerical and analytical results.

We note that for the same parameter values, but for $B = 0$, elliptic fixed points do not exist, and the effective potential has simply the form of a sech^2 barrier, as mentioned above (see also Ref. [12]). In this case, starting from the same initial position, $x_0 = -5$, and for $\phi = 0.1$ (corresponding to $\phi_c = \sqrt{2\Delta W} \approx 0.1$), we find that the trapping time is $t \approx 320$, i.e., almost half of the one that was when the nonlinearity steps were present (results not shown here). This observation, along with the results presented in the previous sections, indicate that nonlinearity steps/barriers are useful towards facilitating or enhancing soliton trapping in such inhomogeneous settings.

IV. RANGE OF VALIDITY OF THE PERTURBATION THEORY AND RADIATION EFFECTS

In the previous sections, we focused on small potential and nonlinearity steps, such that $V_R \sim \epsilon \ll 1$ and $\alpha_R/\alpha_L \sim 1$ (for $\mu_L = 1$ and $V_L = 0$). Nevertheless, for the shake of completeness, here we will also briefly address the case of relatively larger potential/nonlinearity steps. Our aim is to investigate the range of validity of our analytical approximation, and also discuss radiation effects associated with this scenario.

The key point of our analytical approach relies on the equivalent particle picture for solitons which, however, is accurate

only in the perturbative regime of small potential and nonlinearity steps. By increasing the amplitude of the latter, however, the soliton behaves more like a wave, rather than a particle: in fact, an incident soliton at such discontinuities, apart from being either transmitted or reflected, emits radiation in the form of sound waves. These sound waves propagate in both regions $x < 0$ and $x > 0$, with the respective velocities of sound, namely $c_s^{(L)} = 1$ for $x < 0$ and $c_s^{(R)} = \sqrt{n_R}$ for $x > 0$ (where n_R is the background density in this region).

To better illustrate the above, we consider a specific example; notice that qualitatively similar results were found in other cases and, thus, pertinent results are not shown here. Our example corresponds to a dark soliton incident from the right towards a single potential and nonlinearity step, in the setting with $B = -(3/2)A$ (cf. Fig. 8), but now for a relatively large value of A, namely $A = 0.25$; corresponding parameter values are $V_L = 0$, $V_R = 0.25$, $\alpha_R/\alpha_L = 0.625$, and $\mu_R = 1.2$. The result is illustrated in the top panel of Fig. 12, where the density profiles of both the soliton and the emitted radiation are shown. In particular, the dotted (blue) line indicates the density of a soliton, at $t = 0$, with an initial location and velocity given by $x_0 = 10$ and $\phi = -0.2c_s^{(L)} = -0.2$, respectively (recall that the speed of sound is $c_s^{(L)} = 1$ for $x < 0$). The solid (red) line shows a snapshot of the transmitted soliton density at $t = 100$; in addition, at the same time, density profiles of the reflected and transmitted radiation are clearly visible (insets in this figure show pertinent close ups).

The bottom panel of Fig. 12 shows a spatiotemporal contour plot illustrating the evolution of the soliton density; in this figure, the emitted radiation is also observed. Notice that in the same panel, the PDE result is compared to the respective ODE one [dashed (white) line], obtained from Eq. (14). In the region $x < 0$, there is an obvious discrepancy between the two, which indicates a failure of our analytical approach for such large potential/nonlinearity steps. In particular, it is clear that the analytical (ODE) approximation underestimates the soliton velocity, since the PDE result shows that after the scattering process, the soliton becomes deeper and, thus, slower. This indicates that the energy and the number of atoms of the soliton and energy are *decreased*; the difference between final and initial values of these quantities is attributed to the emitted radiation (which is now stronger, as compared to the one corresponding to small potential and nonlinearity steps). In fact, this radiation facilitates the soliton to adapt (decrease) its phase jump, as the soliton is "forced" to evolve on top of a significantly decreased background density. Obviously, the radiation disperses eventually over time.

To quantitatively study the emission of radiation, we focus on the above mentioned configuration with $B = -(3/2)A$, and calculate numerically the renormalized soliton energy E_s and number of atoms N_s [63, 64] for different values of the amplitude A of the potential step; the initial data for the soliton are kept fixed ($x_0 = 10$ and $\phi = -0.2$, i.e., the soliton moves from right to left). Since the background density here is spatially dependent, we rephrase the defintion of E_s and N_s
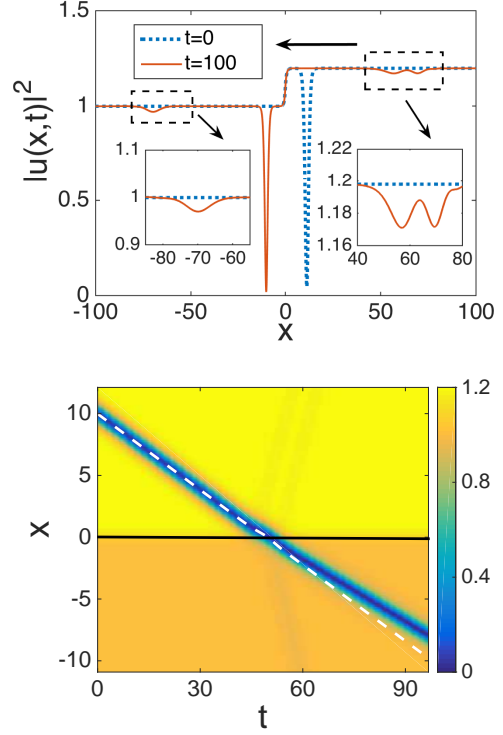

FIG. 12: (Color online) Top panel: background density density profile $|u|^2$ in the presence of a large potential and nonlinearity step, for $A = 0.25$, $B = -(3/2)A = -0.375$, corresponding to $V_L = 0$, $V_R = 0.25$, $\alpha_R/\alpha_L = 0.625$, and $\mu_L = 1$. Dotted (blue) line depicts the density of a soliton at $t = 0$, with initial location $x_0 = 10$ and velocity $\phi = -0.2$, while solid (red) line shows the density of the soliton, as well as the densities of the reflected and transmitted radiation at $t = 100$; insets show close ups of the radiation profiles. Bottom panel: contour plot showing the evolution of the dark soliton density; dashed (white) line depicts the ODE result [cf. Eq. (14)].

as follows:

$$E_s = \frac{1}{2} \int_{x_0-2\xi}^{x_0+2\xi} \left\{ \left| \frac{\partial u}{\partial x} \right|^2 + \left[|u|^2 - n(x) \right]^2 \right\} dx, \quad (34)$$

$$N_s = \int_{x_0-2\xi}^{x_0+2\xi} \left[n(x) - |u|^2 \right] dx, \quad (35)$$

where $n(x)$ is the background density, given by Eq. (19). Here, following Ref. [57], this calculation is performed across the soliton region, indicatively defined to be $x_0 \pm 2\xi$; however E_s in the above expression doesn't represent the actual energy of the soliton (given the explicit spatial variation of $n(x)$) but rather is intended as a diagnostic tool that factors out the contribution of the background field within the domain of integration for each time step. The quantities E_s and N_s, normalized to their corresponding initial values, are shown as functions of time in the top panel of Fig. 13, for three different values of the potential step: $A = 0.01$ [solid (blue) line], $A = 0.15$ [dotted (orange) line], and $A = 0.25$ [dashed (yellow) line].

As shown in the figure, our diagnostic quantities assume constant values before and after the scattering of the soliton
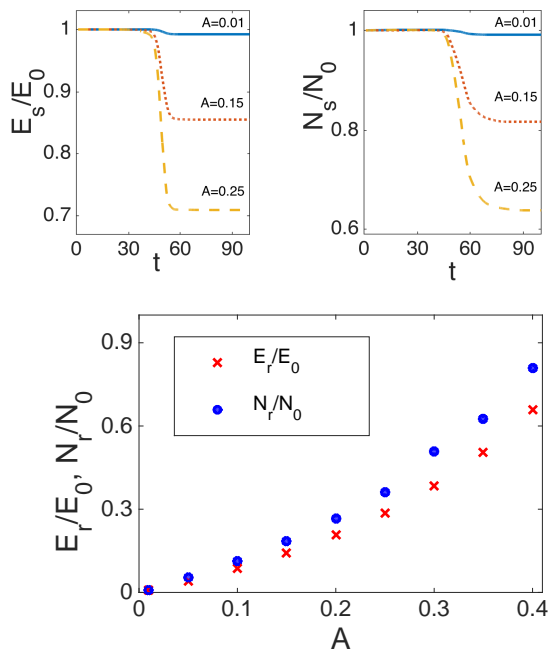
FIG. 13: (Color online) Results for the configuration with $B = -(3/2)A$, for a soliton moving from left to right and scattered (for $t \approx 45$) at the potential/nonlinearity steps. Top panels: normalized soliton energy (left) and number of atoms (right) as functions of time, for $A = 0.01$ ($B = -0.015$, $V_R = 0.01$, $\alpha_R/\alpha_L = 0.985$, cf. solid (blue) line), $A = 0.15$ ($B = -0.225$, $V_R = 0.15$ and $\alpha_R/\alpha_L = 0.775$, cf. dotted (red) line), and $A = 0.25$ ($B = -0.375$, $V_R = 0.25$ and $\alpha_R/\alpha_L = 0.625$, cf. dashed (yellow) line); in all cases, $V_L = 0$ and $\mu_L = 1$, while the initial soliton position and velocity are $x_0 = 10$ and $\phi = -0.2$. Bottom panel: normalized energy [(red) crosses] and number of atoms [(blue) points] of the emitted radiation, at $t = 100$, as functions of the potential step A.

(for $t \approx 45$) at the potential and nonlinearity steps. In all cases, it is observed that the values of E_s/E_0 and N_s/N_0 are decreased after the soliton scattering. In particular, for $A = 0.01$, which is the value used in the previous section, the soliton energy is decreased by $\approx 0.8\%$ and the number of atoms by $\approx 0.9\%$. Obviously, such changes are very small, and result in a negligible amount of emitted radiation. Thus, in this regime, perturbation theory can accurately capture the soliton dynamics, as was demonstrated in the previous section.

However, a significant increase of the value of A, results in corresponding significant decreased values of E_s/E_0 and N_s/N_0 after the soliton scattering: indeed, for $A = 0.15$ the soliton energy and number of atoms decrease by $\approx 15\%$ and $\approx 18\%$, respectively, while for $A = 0.25$ (which is the value used in Fig. 12) the corresponding percentage changes are $\approx 30\%$ and $\approx 36\%$. It is clear that in these cases the emitted radiation is quite strong, and cannot be neglected; this, in turn, results in the failure of the analytical approximation, as discussed above in the example of Fig. 12.

For the considered configuration with $B = -(3/2)A$, we

can draw that then the energy E_r and number of atoms N_r of the emitted radiation are given by:

$$E_r = E_0 - E_s, \quad N_r = N_0 - N_s, \qquad (36)$$

where, as before, E_s (N_s) is the soliton energy (number of atoms) after the scattering of the soliton at the potential/nonlinearity steps while E_0 (N_0) are corresponding initial values.

It is also interesting to find the energy and number of atoms of the emitted radiation as a function of the potential step A – again for the configuration with $B = -(3/2)A$, and for a soliton moving from larger to smaller background density, i.e., from right to left. The respective results, for E_r/E_0 [(red) crosses] and N_r/N_0 [(blue) points], are shown in the bottom panel of Fig. 13. Note that for this plot, E_r and N_r were found numerically at a sufficiently large time, namely at $t = 100$, so that the emitted radiation was well separated from the scattered soliton (see also the example shown in Fig. 12). It is observed that, as long as the potential step takes values $A \lesssim 0.1$, the energy and number of atoms of the radiation remain small, of the order of $\approx 10\%$ of the values of the respective initial soliton quantities. Obviously, soliton dynamics in this regime can be well described in the framework of our analytical approximation. On the other hand, outside this perturbative regime, radiation becomes significantly stronger; for instance, for $A = 0.25$, the energy and number of atoms of the emitted radiation become larger than 30% of the respective initial soliton quantities, as was also found in the top panels of Figs. 12 [cf. dashed (yellow) lines] and Fig. 13. Therefore, for such a strong radiation emission, the failure of the ODE picture is naturally expected, cf. bottom panel of Fig. 13.

V. DISCUSSION AND CONCLUSIONS

We have studied matter-wave dark solitons near linear potential and nonlinearity steps, superimposed on a box-like potential that was assumed to confine the atomic Bose-Einstein condensate. The formulation of the problem finds a direct application in the context of nonlinear optics: the pertinent model can be used to describe the evolution of beams, carrying dark solitons, near interfaces separating optical media with different linear refractive indices and different defocusing Kerr nonlinearities.

Assuming that the potential/nonlinearity steps were small, we employed perturbation theory for dark solitons to show that, in the adiabatic approximation, solitons behave as equivalent particles moving in the presence of an effective potential. The latter was found to exhibit various forms, ranging from simple tanh-shaped steps – for a spatially homogeneous scattering length (or same Kerr nonlinearity, in the context of optics) – to more complex forms, featuring extrema, i.e., hyperbolic and elliptic fixed points in the associated dynamical system – in the presence of steps in the scattering length (different Kerr nonlinearities).

In the latter case, we found that stationary soliton states do exist at the fixed points. Using a Bogoliubov-de Gennes (BdG) analysis, we showed that these states are unstable: dark

solitons at the hyperbolic fixed points have a pair of unstable real eigenvalues, while those at the elliptic fixed points have a complex eigenfrequency quartet, dictating a purely exponential or an oscillatory instability, respectively. The case of the oscillatory instability was studied in detail, and it was shown that, in fact, the elliptic point in the effective particle picture actually behaves as an unstable spiral in the framework of the Gross-Pitaevskii model (and in accordance to the BdG analysis). We also used an analytical approximation to determine the real and imaginary parts of the relevant eigenfrequencies as functions of the nonlinearity step strength. The analytical predictions were found to be in good agreement with corresponding numerical findings obtained in the framework of the BdG analysis.

We then studied systematically soliton dynamics, for a variety of parameter values corresponding to all possible forms of the effective potential. Adopting the aforementioned equivalent particle picture, we found analytically necessary conditions for soliton reflection at, or transmission through the potential and nonlinearity steps: these correspond to initial soliton velocities smaller or greater to the energy of the effective steps/barriers predicted by the perturbation theory and the equivalent particle picture.

We also investigated the possibility of soliton (quasi-) trapping, for initial conditions corresponding to the incoming, stable manifolds of the hyperbolic fixed points (which exist only for inhomogeneous nonlinearities). In the context of optics, such a trapping can be regarded as the formation of surface dark solitons at the interface between dielectrics of different refractive indices. We found that trapping is possible, but only for a finite time. This effect can be understood by the fact that stationary solitons at the hyperbolic fixed points are unstable, as was corroborated by the BdG analysis. Thus small perturbations (at the PDE level) eventually cause the departure of the solitary wave from the relevant fixed points. Nevertheless, it should be pointed out that the time of soliton quasi-trapping was found to be of the order of $600\sqrt{2}\xi/c_S$ in physical units; thus, typically, for a healing length ξ of the order of a micron and a speed of sound c_s of the order of a millimeter-per-second, trapping time may be of the order of ≈ 850 ms. This indicates that such a soliton quasi-trapping effect may be observed in real experiments. Note that in all scenarios (reflection, transmission, quasi-trapping) our analytical predictions were found to be in very good agreement with direct numerical simulations in the framework of the original Gross-Pitaevskii model.

We have also extended our considerations to study cases involving two potential and nonlinearity steps, that are combined so as to form corresponding rectangular barriers. Reflection, transmission and quasi-trapping of solitons in such cases were studied too, again with a very good agreement between analytical and numerical results. In this setting, special attention was paid to the limiting case of infinitesimally small distance between the adjacent potential/nonlinearity steps that form the barriers. In this case, we found that, due to a pitchfork bifurcation, the stability of the fixed point of the effective potential at the barrier center changes: out of two hyperbolic and one elliptic fixed point, a hyperbolic fixed point emerges,

and the potential rectangular barrier is reduced to a delta-like impurity. The latter is described by a sech^2 effective potential, in accordance with the analysis of earlier works [8, 12, 13].

Finally, we also studied soliton scattering at relatively large potential/nonlinearity steps. Our investigation reveals that, in this case, soliton scattering results in significant emission of radiation in both sides of the interface. We found that the soliton's number of atoms and energy decrease when the soliton is scattered at regions of lower background density. The number of atoms and energy of the radiation was thus found to be equal to the difference between initial and final values of the soliton number of atoms and energy. We have also found that our analytical approximation, based on the equivalent particle picture remains accurate as long as the percentage difference between potential/nonlinearity steps is up to 10%; in such a case the radiation is actually negligible. Nevertheless, for larger than 10% values, the emission of radiation is stronger; this effect can not be captured by our analytical approach, which evidently fails in such a nonperturbative regime.

Our methodology and results pose a number of interesting questions for future studies. First, it would be interesting to investigate how our perturbative results change as the potential/nonlinearity steps or barriers become larger, and/or attain more realistic shapes (including steps bearing finite widths, as well as Gaussian barriers – cf., e.g., recent work of Ref. [16]). In the same context, a systematic numerical – and, possibly, also analytical – study of the radiation of solitons during reflection or transmission (along the lines, e.g., of Ref. [57]) should also provide a more complete picture in this problem. Furthermore, a systematic study of settings involving multiple such steps/barriers, and an investigation of the possibility of soliton trapping therein, would be particularly relevant. In such settings, investigation of the dynamics of moving steps/barriers could find direct applications to fundamental studies relevant, e.g., to superfluidity (see, for instance, Ref. [22]), transport of BECs [23], and even Hawking radiation in analog black hole lasers implemented with BECs [68]. Finally, extension of our analysis to higher-dimensional settings, would also be particularly challenging: first, in order to investigate transverse excitation effects that are not captured within the quasi-1D setting, and second to study similar problems with vortices and other vortex structures. See, e.g., Ref. [69] for a summary of relevant studies in higher-dimensional settings, and Ref. [70] for a recent example of manipulation/control of vortex patterns and their formation via Gaussian barriers, motivated by experimentally accessible laser beams.

[1] Yu. S. Kivshar and B. A. Malomed, Rev. Mod. Phys. **61**, 763 (1989).

[2] I. M. Lifshitz and A. M. Kosevich, Rep. Prog. Phys. **29**, 217 (1966).

[3] I. Ianni, S. L. Coz, and J. Royer, arXiv:1506.03761.

[4] A. M. Kosevich, Physica D **41**, 253 (1990).

[5] X. D. Cao and B. A. Malomed, Phys. Lett. A **206**, 177 (1995).

[6] R. H. Goodman, P. J. Holmes, and M. I. Weinstein, Physica D **192**, 215 (2004).

[7] J. Holmer, J. Marzuola, and M. Zworski, Comm. Math. Phys. **274**, 187 (2007); J. Holmer, J. Marzuola, and M. Zworski, J. Nonlin. Sci. **17**, 349 (2007).

[8] V. V. Konotop, V. M. Pérez-García, Y.-F. Tang, and L. Vázquez, Phys. Lett. A **236**, 314 (1997).

[9] L. P. Pitaevskii and S. Stringari, *Bose-Einstein Condensation* (Oxford University Press, Oxford, 2003).

[10] P. G. Kevrekidis, D. J. Frantzeskakis, and R. Carretero-González (eds.), *Emergent Nonlinear Phenomena in Bose-Einstein Condensates: Theory and Experiment* (Springer-Verlag, Berlin, 2008); R. Carretero-González, D. J. Frantzeskakis, and P. G. Kevrekidis, Nonlinearity **21**, 139 (2008).

[11] V. S. Bagnato, D. J. Frantzeskakis, P. G. Kevrekidis, B. A. Malomed and D. Mihalache, Rom. Rep. Phys. **67**, 5 (2015).

[12] D. J. Frantzeskakis, G. Theocharis, F. K. Diakonos, P. Schmelcher, and Yu. S. Kivshar, Phys. Rev. A **66**, 053608 (2002).

[13] N. Bilas and N. Pavloff, Phys. Rev. A **72**, 033618 (2005).

[14] N. Bilas and N. Pavloff, Phys. Rev. Lett. **95**, 130403 (2005).

[15] G. Herring, P. G. Kevrekidis, R. Carretero-González, B. A. Malomed, D. J. Frantzeskakis, and A. R. Bishop, Phys. Lett. A **345**, 144 (2005).

[16] I. Hans, J. Stockhofe, and P. Schmelcher, Phys. Rev. A **92**, 013627 (2015).

[17] T. Ernst and J. Brand, Phys. Rev. A **81**, 033614 (2010).

[18] C. Lee and J. Brand, Europhys. Lett. **73**, 321 (2006).

[19] J. L. Helm, T. P. Billam, and S. A. Gardiner, Phys. Rev. A **85**, 053621 (2012).

[20] A. D. Martin and J. Ruostekoski, New J. Phys. **14**, 043040 (2012).

[21] Y. Nogami and F. M. Toyama, Phys. Lett. A **184**, 245-250 (1994).

[22] P. Engels and C. Atherton, Phys. Rev. Lett. **99**, 160405 (2007).

[23] D. Dries, S. E. Pollack, J. M. Hitchcock, and R. G. Hulet, Phys. Rev. A **82**, 033603 (2010).

[24] J. Cuevas, P. G. Kevrekidis, B. A. Malomed, P. Dyke, and R. G. Hulet, New J. Phys. **15**, 063006 (2013).

[25] A. L. Marchant, T. P. Billam, T. P. Wiles, M. M. H. Yu, S. A. Gardiner, and S. L. Cornish, Nat. Com. **4**, 1865 (2013).

[26] V. Achilleos, P. G. Kevrekidis, V. M. Rothos, and D. J. Frantzeskakis, Phys. Rev. A **84**, 053626 (2011).

[27] A. Álvarez, J. Cuevas, F. R. Romero, C. Hamner, J. J. Chang, P. Engels, P. G. Kevrekidis, and D. J. Frantzeskakis, J. Phys. B: At. Mol. Opt. Phys. **46**, 065302 (2013).

[28] G. Theocharis, P. Schmelcher, P. G. Kevrekidis, and D. J. Frantzeskakis, Phys. Rev. A **72**, 033614 (2005).

[29] S. Middelkamp, P. G. Kevrekidis, D. J. Frantzeskakis and P. Schmelcher, Phys. Lett. A **373**, 262268 (2009).

[30] Y. V. Kartashov, B. A. Malomed, and L. Torner, Rev. Mod. Phys. **83**, 247 (2011).

[31] F. Kh. Abdullaev and M. Salerno, J. Phys. B: At. Mol. Opt. Phys. **36**, 2851 (2003).

[32] M. I. Rodas-Verde, H. Michinel, and V. M. Pérez-García, Phys. Rev. Lett. **95**, 153903 (2005); A. V. Carpentier, H. Michinel, M. I. Rodas-Verde, and V. M. Pérez-García, Phys. Rev. A **74**, 013619 (2006).

[33] F. Tsitoura, P. Krüger, P. G. Kevrekidis, and D. J. Frantzeskakis, Phys. Rev. A, **91**, 033633 (2015).

[34] G. Theocharis, P. Schmelcher, P. G. Kevrekidis, and D. J. Frantzeskakis, Phys. Rev. A **74**, 053614 (2006); J. Garnier and F. Kh. Abdullaev, *ibid.* **74**, 013604 (2006); P. Niarchou, G. Theocharis, P. G. Kevrekidis, P. Schmelcher, and D. J. Frantzeskakis, *ibid.* **76**, 023615 (2007).

[35] C. Wang, K.J.H. Law, P. G. Kevrekidis, and M. A. Porter, Phys. Rev. A **87**, 023621 (2013).

[36] G. Dong, B. Hu, and W. Lu, Phys. Rev. A **74**, 063601 (2006).

[37] H. Sakaguchi and B. A. Malomed, Phys. Rev. A **81**, 013624 (2010);

[38] S. Holmes, M. A. Porter, P. Krüger, and P. G. Kevrekidis, Phys. Rev. A **88**, 033627 (2013).

[39] K. Hizanidis, Y. Kominis, and N. K. Efremidis, Opt. Express **16**, 18296 (2008).

[40] R. Marangell, C.K.R.T. Jones, and H. Susanto, Nonlinearity **23**, 2059 (2010).

[41] R. Marangell, H. Susanto, and C.K.R.T. Jones, J. Diff. Eq. **253**, 1191 (2012).

[42] C. Wang, P. G. Kevrekidis, T. P. Horikis, and D. J. Frantzeskakis, Phys. Lett. A **374**, 3863 (2010); T. Mithun, K. Porsezian, and B. Dey, Phys. Rev. E **88**, 012904 (2013).

[43] F. Pinsker, N. G. Berloff, and V. M. Pérez-García, Phys. Rev. A **87**, 053624 (2013).

[44] A. Balaz, R. Paun, A. I. Nicolin, S. Balasubramanian, and R. Ramaswamy, Phys. Rev. A **89**, 023609 (2014).

[45] T. Kaneda and H. Saito, Phys. Rev. A **90**, 053632 (2014).

[46] A. Weller, J. P. Ronzheimer, C. Gross, J. Esteve, M. K. Oberthaler, D. J. Frantzeskakis, G. Theocharis, and P. G. Kevrekidis, Phys. Rev. Lett. **101**, 130401 (2008); S. Stellmer, P. Soltan-Panahi, S. Dörscher, M. Baumert, E.-M. Richter, J. Kronjäger, K. Bongs, and K. Sengstock, Nat. Phys. **4**, 496 (2008); S. Stellmer, C. Becker, P. Soltan-Panahi, E.-M. Richter, S. Dörscher, M. Baumert, J. Kronjäger, K. Bongs, and K. Sengstock, Phys. Rev. Lett. **101**, 120406 (2008); G. Theocharis, A. Weller, J. P. Ronzheimer, C. Gross, M. K. Oberthaler, P. G. Kevrekidis, and D. J. Frantzeskakis, Phys. Rev. A **81**, 063604 (2010).

[47] B. T. Seaman, L. D. Carr, and M. J. Holland, Phys. Rev. A, **71**, 033609 (2005).

[48] L. D. Carr, R. R. Miller, D. R. Bolton, and S. A. Strong, Phys. Rev. A **86**, 023621 (2012).

[49] S. Inouye, M. R. Andrews, J. Stenger, H. J. Miesner, D. M.

Stamper-Kurn, and W. Ketterle, Nature (London) **392**, 151 (1998); J. Stenger, S. Inouye, M. R. Andrews, H.-J. Miesner, D. M. Stamper-Kurn, and W. Ketterle, Phys. Rev. Lett. **82**, 2422 (1999); J. L. Roberts, N. R. Claussen, J. P. Burke, Jr., C. H. Greene, E. A. Cornell, and C. E.Wieman, *ibid.* **81**, 5109 (1998); S. L. Cornish, N. R. Claussen, J. L. Roberts, E. A. Cornell, and C. E. Wieman, *ibid.* **85**, 1795 (2000).

[50] F. K. Fatemi, K. M. Jones, and P. D. Lett, Phys. Rev. Lett. **85**, 4462 (2000); M. Theis, G. Thalhammer, K. Winkler, M. Hellwig, G. Ruff, R. Grimm, and J. H. Denschlag, *ibid.* **93**, 123001 (2004).

[51] A. C. Newell and J. V. Moloney, *Nonlinear Optics* (Addison-Wesley, Redwood City, CA, 1992).

[52] A. B. Aceves, J. V. Moloney, and A. C. Newell, J. Opt. Soc. Am. B **5**, 559 (1988); Phys. Lett. A **129**, 231 (1988); Phys. Rev. A **39**, 1809 (1989); *ibid.* **39**, 1828 (1989).

[53] Yu. S. Kivshar, A. M. Kosevich, and O. A. Chubykalo, Phys. Rev. A **41**, 1677 (1990).

[54] Yu. S. Kivshar and M. L. Quiroga-Teixeiro, Phys. Rev. A **48**, 4750 (1993).

[55] Y. Kominis and K. Hizanidis, Phys. Rev. Lett. **102**, 133903 (2009).

[56] H. Sakaguchi and M. Tamura, J. Phys. Soc. Jpn. **74**, 292 (2005).

[57] N. G. Parker, N. P. Proukakis, M. Leadbeater, and C. S. Adams, J. Phys. B: At. Mol. Opt. Phys. **36**, 2891 (2003); N. G. Parker, N. P. Proukakis, C. F. Barenghi, and C. S. Adams, J. Phys. B: At. Mol. Opt. Phys. **37**, S175 (2004).

[58] N. P. Proukakis, N. G. Parker, D. J. Frantzeskakis, and C. S. Adams, J. Opt. B: Quantum Semiclass. Opt. **6**, S380 (2004).

[59] H. Sakaguchi, Laser Phys. **16**, 340 (2006).

[60] M. Kurzke, J.L. Marzuola and D. Spirn, arXiv:1510.08093 (2015).

[61] R. Folman, P. Krüger, J. Denschlag, J. Schmiedmayer, and C. Henkel, Adv. At. Mol. Opt. Phys. **48**, 263 (2002).

[62] L. D. Carr, C. W. Clark, and W. P. Reinhardt, Phys. Rev. A **62**, 063610 (2000).

[63] Yu. S. Kivshar and X. Yang, Phys. Rev. E **49**, 1657 (1994).

[64] D. J. Frantzeskakis, J. Phys. A: Math. Theor. **43**, 213001 (2010).

[65] M. J. Ablowitz, S. D. Nixon, T. P. Horikis, and D. J. Frantzeskakis, Proc. R. Soc. A **2133**, 2597 (2011).

[66] D. E. Pelinovsky and P. G. Kevrekidis, ZAMP **59**, 559 (2008).

[67] A. S. Rodrigues, P. G. Kevrekidis, M. A. Porter, D. J. Frantzeskakis, P. Schmelcher, and A. R. Bishop, Phys. Rev. A **78**, 013611 (2008).

[68] J. Steinhauer, Nat. Phys. **10**, 864 (2014).

[69] P. G. Kevrekidis, D. J. Frantzeskakis, and R. Carretero-González, *The defocusing Nonlinear Schrödinger Equation: From Dark Solitons to Vortices and Vortex Rings* (SIAM, Philadelphia, 2015).

[70] B. Gertjerenken, P. G. Kevrekidis, R. Carretero-González, and B. P. Anderson, Phys. Rev. A **93**, 023604 (2016).